

# Coherent Lattice Vibrations in Carbon Nanotubes

Y. S. Lim,<sup>1,2</sup> K. J. Yee,<sup>3</sup> J. H. Kim,<sup>3</sup> J. Shaver,<sup>1,5</sup> E. H. Haroz,<sup>1,5</sup> J. Kono,<sup>1,5</sup>

S. K. Doorn,<sup>4</sup> R. H. Hauge,<sup>5</sup> and R. E. Smalley<sup>5</sup>

<sup>1</sup>Department of Electrical and Computer Engineering, Rice University, Houston, Texas 77005, USA

<sup>2</sup>Department of Applied Physics, Konkuk University, Chungju, Chungbuk 380-701, Republic of Korea

<sup>3</sup>Department of Physics, Chungnam National University, Daejeon 305-764, Republic of Korea

<sup>4</sup>Division of Chemistry, Analytical Chemistry Science,

Los Alamos National Laboratory, Los Alamos, New Mexico 87545, USA

<sup>5</sup>Carbon Nanotechnology Laboratory, Rice University, Houston, Texas 77005, USA

(Dated: April 15, 2024)

We have generated and detected the radial-breathing mode of coherent lattice vibrations in single-walled carbon nanotubes using ultrashort laser pulses. Because the band gap is a function of diameter, these diameter oscillations cause ultrafast band gap oscillations, modulating interband excitonic resonances at the phonon frequencies (3–9 THz). Excitation spectra show a large number of pronounced peaks, mapping out chirality distributions in great detail.

Electrons, phonons, and their mutual interaction determine most of the properties of crystalline solids [1]. Optical and electrical properties, in particular, are almost entirely dominated by these two fundamental excitations and it is the subtle interplay between them that gives rise to phenomena such as the Franck-Condon principle and superconductivity. With the advent of ultrafast spectroscopy, one can probe electronic and vibrational dynamics in real time [2, 3]. Single-walled carbon nanotubes (SWNTs), with their uniquely-simple crystal structures and chirality-dependent electronic and vibrational states, provide a one-dimensional playground for studying the dynamics and interactions of electrons and phonons. Recent CW optical studies of SWNTs [4, 5, 6, 7, 8, 9, 10, 11, 12, 13, 14] have produced a world of intriguing phenomena, including phonon-assisted photoluminescence, strongly bound excitons, and chirality-dependent resonant Raman scattering (RRS) { results of interaction between excited electronic/excitonic states and phonons [15, 16, 17, 18, 19, 20, 21].

Here we show a real-time observation of lattice vibrations in SWNTs. Using pump-probe spectroscopy we observed coherent phonons (CPs) in individual SWNTs, corresponding to the radial-breathing mode (RBM). The observed RBMs were found to correspond exactly to those seen by CW RRS for the same sample but with narrower phonon linewidths, no photoluminescence signal or Rayleigh scattering background to obscure features, and excellent resolution allowing normally blended peaks to appear as distinct features. Additionally, differences in the RBM intensity of families of SWNTs were observed between CP and RRS. Finally, when viewing the excitation profiles of several RBMs, we found a two-peak resonance, which we attribute to this technique acting as a modulation spectroscopy; i.e., we are observing the first derivative of the interband excitonic absorption peak.

The sample used in this study was a micelle-suspended SWNT solution with a diameter range of 0.7–1.3 nm. The SWNTs were individually suspended with sodium

dodecyl sulfate in D<sub>2</sub>O [4] in a quartz cell with an optical path length of 1 mm. We performed degenerate pump-probe measurements at room temperature using

50 fs pulses at a repetition rate of 89 MHz from a mode-locked Ti:Sapphire laser with an average pump power of 20 mW. We tuned the center wavelength in 5-nm steps from 710 nm to 860 nm (1.75–1.43 eV) by controlling the slit between the intracavity prism pair in the Ti:Sapphire laser. In the CW RRS experiments on the same sample, the excitation source was a Ti:Sapphire laser with a power of 15 mW at the sample. Signal collection was done using a triple monochromator and CCD camera.

Figure 1(a) shows coherent phonon oscillations in SWNTs excited at different pump photon energies. The amplitude of oscillations in terms of normalized differential transmission was  $\sim 10^{-4}$  near zero delay. Each trace consists of a superposition of multiple oscillation modes with different frequencies, exhibiting a strong beating pattern. The beating pattern sensitively changes with the photon energy, implying that the CP oscillations are dominated by RBMs which are resonantly enhanced by pulses commensurate with their unique electronic transitions, as is the case in CW Raman scattering. The dephasing time of the dominant CP oscillations was  $\sim 5$  ps.

To determine the frequencies of the excited lattice vibrations, we took a fast Fourier transform (FFT) of the time-domain oscillations to produce CP spectra [Fig. 1(b)]. For comparison, we show CW RRS spectra [Fig. 1(c)] for the same sample. The CP spectra [Fig. 1(b)] are seen to cluster into three distinct regions, similar to CW RRS [7], as shown in Fig. 1(c). The main peak positions coincide between Fig. 1(b) and Fig. 1(c), indicating that the oscillations seen in Fig. 1(a) are indeed due to the RBM of coherent lattice vibrations. However, upon close examination, we find a few noticeable differences between the CP data and CW RRS data: i) unresolved shoulder features in RRS are seen as resolved peaks in the CP spectra due to narrower linewidths, ii) there are different intensity distributions

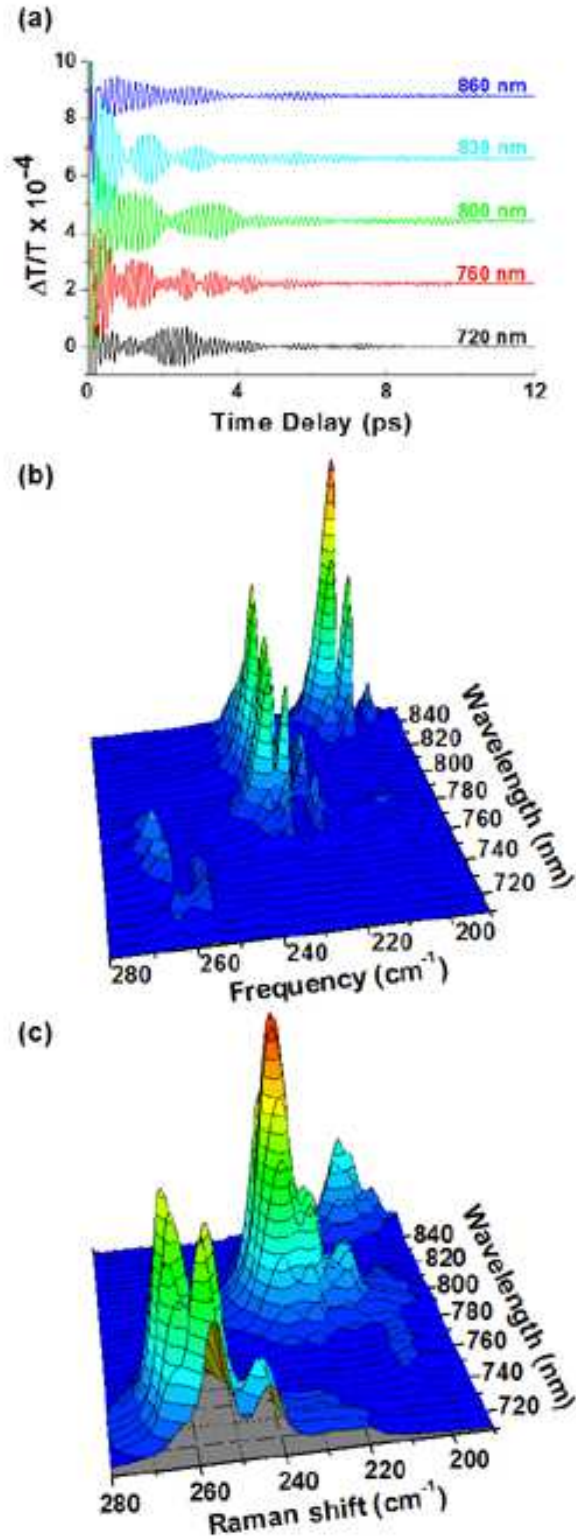


FIG. 1: (a) Coherent phonon oscillations excited and measured at five different photon energies. (b) A 3D plot of the Fast Fourier Transform of coherent phonon oscillations obtained over a photon energy range of 710–850 nm (1.746–1.459 eV) with a 5-nm step size. (c) A 3D plot of resonant Raman scattering over an excitation energy range of 710–850 nm (1.746–1.459 eV) with a 5-nm step size.

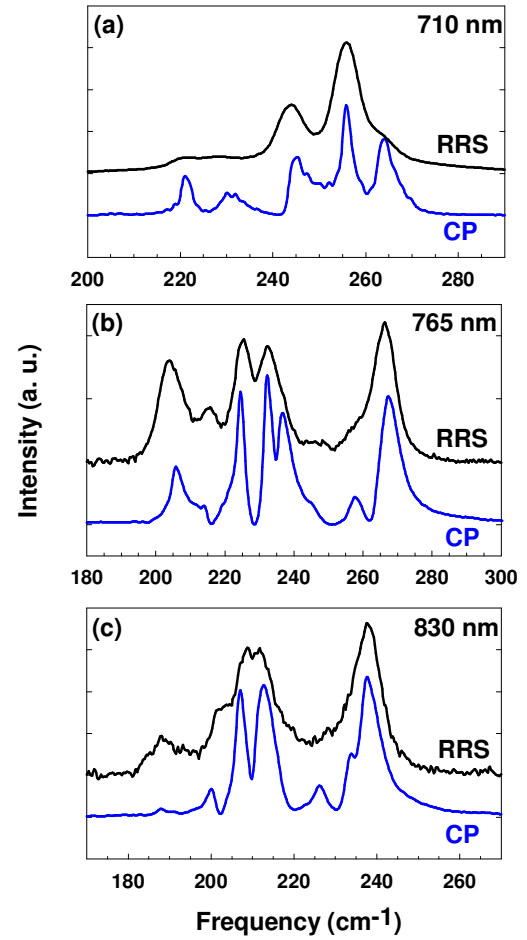


FIG. 2: Phonon spectra using three different photon energies obtained from resonant Raman scattering (RRS) and coherent phonon (CP) measurement. Coherent phonon data exhibits dramatically narrower line widths.

among the strongest peaks in the three distinct regions, and iii) the CP spectra show a surprising double-peak dependence on the photon energy. These differences are discussed in more depth in the following.

Figures 2(a)–2(c) present direct comparison between CP spectra and CW RRS spectra. Here, the CP spectra obtained with different wavelengths are overlaid on the equivalent RRS spectra taken at the same wavelengths of 710 nm (1.746 eV), 765 nm (1.621 eV), and 830 nm (1.494 eV), respectively. There is overall agreement between the two spectra in each figure. However, it is clear that many more features are resolved in the CP data. The narrower line widths in the CP data make it possible to resolve blended peaks in the RRS data. With less overlap among the close-by peaks, more precise determination of line positions is possible. Through peak fitting using Lorentzians, we have identified and successfully assigned 18 RBMs in the CP spectra over the 1.44–1.75 eV (710–860 nm) photon energy range.

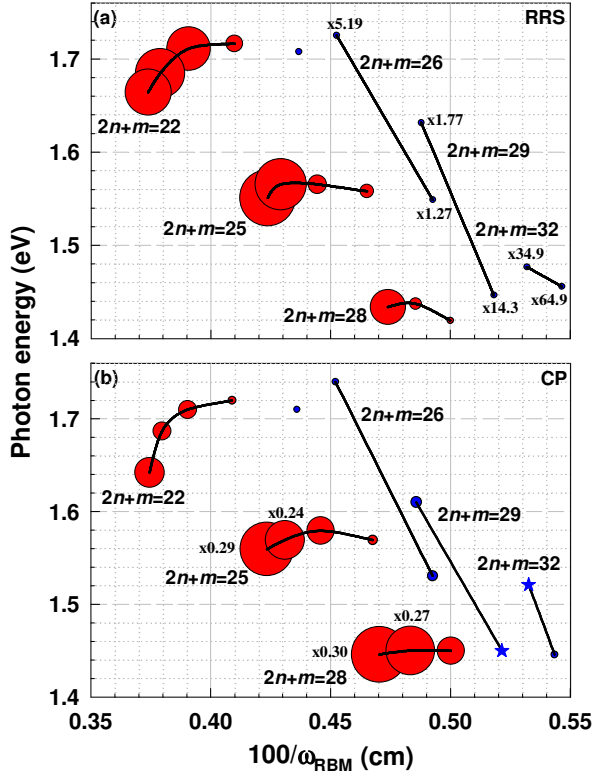


FIG. 3: (a) Raman intensity and (b) coherent phonon signal as a function of excitation energy and  $100/\omega_{\text{RBM}}$ , where  $\omega_{\text{RBM}}$  is the phonon frequency. Red (blue) circles denote nanotubes that satisfy  $(n, m) \bmod 3 = 1$  ( $+1$ ). The black lines connect members of the same  $(2n+m)$  family. The diameter of the circles is proportional to measured intensities [26]. The blue stars in (b) indicate chiralities with large uncertainty in their determined excitonic energies and coherent phonon signal.

The measured average linewidth of RBMs of semiconducting nanotubes obtained from CP measurements is approximately  $3 \text{ cm}^{-1}$ . Those measured in this study for HiPco material using CW RRS and in other high-resolution CW RRS experiments [22] for the outer walls of double-walled carbon nanotubes, individual SWNTs on substrates, and individual SWNTs dispersed in solution were approximately  $5\text{--}6 \text{ cm}^{-1}$ . This observation is consistent with results of previous studies on coherent phonons in semiconductors [23, 24] and clearly indicates that the two techniques are sensitive to different dynamical quantities. CP data contains information on how impulsively-generated transient coherent phonons decay. Once the coherent phonons are generated, their decay processes are most likely to be through disappearance into lower-frequency phonon modes by anharmonicity [3, 25], independent of any electronic states or processes. Raman linewidths are affected by the electronic states involved as well as electron-phonon interactions. This makes CP an ideal method for phonon spectroscopy with precise determination of both frequencies and decay times.

Figure 3 summarizes the observed various RBMs both for CW Raman scattering [Fig. 3(a)] and coherent phonons [Fig. 3(b)] [26]. The dependence of CP signal strength as a function of photon energy and phonon frequency exhibits several of the same trends both predicted theoretically [17, 18, 19, 20, 21] and measured experimentally [7, 14] by CW Raman scattering intensity as a function of excitation energy and Raman shift. First, when exciting the second excitonic transition for an individual semiconducting SWNT,  $E_{22}$ ,  $(n, m) \bmod 3 = 1$  nanotubes have markedly stronger signal than  $(n, m) \bmod 3 = +1$  nanotubes. Second, within a  $(2n+m)$  nanotube family, signal strength increases from nanotubes with large chiral angles (near-arm chair) to nanotubes with small or 0 chiral angle (zigzag). However, the two techniques diverge in similarity when comparing the overall strength in signal. Namely, in Raman scattering, signal strength decreases as  $(2n+m) = \text{constant}$  increases whereas CP signal increases with increasing  $(2n+m) = \text{constant}$ . We currently have no theoretical model to explain this striking difference between CP measurements and RRS, and it is thus open for further studies.

Finally, we discuss how the generation of CPs of RBMs modifies the electronic structure of SWNTs and how it can be detected as temporal oscillations in the transmittance of the probe beam. The RBM is an isotropic vibration of the nanotube lattice in the radial direction, i.e., the diameter ( $d_t$ ) periodically oscillates at frequency  $\omega_{\text{RBM}}$ . This causes the band gap  $E_g$  to also oscillate at  $\omega_{\text{RBM}}$  [see Fig. 4(a)] because  $E_g$  directly depends on the nanotube diameter (roughly  $E_g \propto 1/d_t$ ). As a result, interband transition energies oscillate in time, leading to ultrafast modulations of optical constants at  $\omega_{\text{RBM}}$ , which naturally explains the oscillations in probe transmittance. Furthermore, these modulations imply that the absorption coefficient at a fixed probe photon energy is modulated at  $\omega_{\text{RBM}}$ . Correspondingly, the photon energy dependence of the CP signal shows a derivative-like behavior, a modulation spectroscopy [27] [see Figs. 4(b) and 4(c)]. We modeled this behavior assuming that the CP signal intensity is proportional to the absolute value of the convoluted integral of the first derivative of a Lorentzian absorption line and a Gaussian probe beam profile. The results, shown as solid lines in Figs. 4(b) and 4(c), successfully reproduce the observed double peaks, whose energy separation changes with the bandwidth of the probe. The symmetric double-peak feature confirms the excitonic nature of the absorption line, in contrast to the asymmetric shape expected from the 1-D van Hove singularity.

In addition to revealing a novel optical process, involving both 1-D excitons and phonons simultaneously, this study opens up a number of new possibilities to study SWNTs. In particular, it has many advantages over conventional CW characterization methods, including i) easy tuning of the center wavelength of the pump

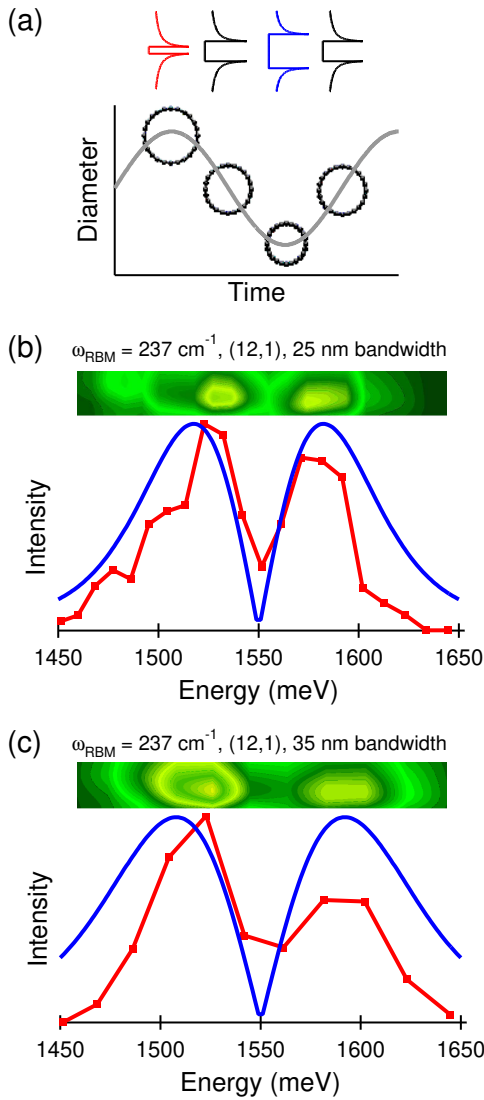


FIG. 4: (a) Time-dependent band gap due to the radial-breathing mode of coherent lattice oscillations. (b) and (c): The photon energy dependence of the coherent phonon signal intensity (both contour and 2D plots) for the (12,1) tube with a probe bandwidth of (b) 25 nm and (c) 35 nm together with theoretical curves (blue solid lines).

pulse, ii) simultaneous excitation of multiple vibrational modes due to the broad spectrum of the exciting pulse, iii) no Rayleigh scattering background at low frequency, iv) no photoluminescence signal, and v) direct measurement of vibrational dynamics including its phase information and dephasing times. The excitonic nature of interband optical excitation manifests itself in the detection process for the CP oscillations by the coupling with the broad spectrum of probe pulses. Furthermore, the expansion of the spectrum of femtosecond pulses into deep mid-infrared and visible ranges will allow us to explore large-diameter carbon nanotubes and metallic car-

bon nanotubes. Finally, the ability of CP measurements to trace the first derivative of the excitonic absorption peaks of specific chirality ( $n,m$ ) will allow in-depth study of the lineshape of these resonances.

YSL acknowledges financial support from Konkuk University. This work was supported in part by the Robert A. Welch Foundation (No. C-1509) and NSF (Nos. DMR-0134058 and DMR-0325474). SKD appreciates the support of the LANL Integrated Spectroscopy Laboratory and partial financial support of this work from the LANL LDRD program. We thank C. Kittrell for helpful discussions and comments.

<sup>y</sup>To whom correspondence should be addressed. Electronic address: kono@rice.edu.

- 
- [1] J. M. Ziman, *Electrons and Phonons* (Oxford University Press, Oxford, 1960).
  - [2] J. Shah, *Ultrafast Spectroscopy of Semiconductors and Semiconductor Nanostructures*, 2nd ed. (Springer, Berlin, 1999).
  - [3] R. Merlin, *Solid State Commun.* 102, 207 (1997).
  - [4] M. J. O'Connell et al., *Science* 297, 593 (2002).
  - [5] S. M. Bachilo et al., *Science* 298, 2361 (2002).
  - [6] S. Zaric et al., *Science* 304, 1129 (2004).
  - [7] S. K. Doorn et al., *Appl. Phys. A* 78, 1147 (2004).
  - [8] H. Telieps et al., *Phys. Rev. Lett.* 93, 177401 (2004).
  - [9] C. Fantini et al., *Phys. Rev. Lett.* 93, 147406 (2004).
  - [10] M. Y. Sfeir et al., *Science* 306, 1540 (2004).
  - [11] F. Wang et al., *Science* 308, 838 (2005).
  - [12] J. Maultzsch et al., *Phys. Rev. B* 72, 241402(R) (2005).
  - [13] A. Jorio et al., *Phys. Rev. B* 71, 075401 (2005).
  - [14] J. Maultzsch et al., *Phys. Rev. B* 72, 205438 (2005).
  - [15] V. Perebeinos et al., *Phys. Rev. Lett.* 94, 027402 (2005).
  - [16] C. Thomsen and S. Reich, in: *Light Scattering in Solids IX*, eds. M. Cardona and R. Merlin (Springer, Berlin, 2006), Chapter 3.
  - [17] V. N. Popov, L. Henrard, and P. Lambin, *Nano Lett.* 4, 1795 (2004); *Phys. Rev. B* 72, 035436 (2005).
  - [18] M. M. M. achon et al., *Phys. Rev. B* 71, 035416 (2005).
  - [19] S. V. Goupalov, *Phys. Rev. B* 71, 153404 (2005).
  - [20] J. Jiang et al., *Phys. Rev. B* 71, 205420 (2005).
  - [21] S. V. Goupalov et al., *Phys. Rev. B* 73, 115401 (2006).
  - [22] F. Simon et al., *Chem. Phys. Lett.* 413, 506 (2005).
  - [23] K. J. Yee et al., *Phys. Rev. Lett.* 88, 105501 (2002).
  - [24] I. H. Lee et al., *J. Appl. Phys.* 93, 4939 (2003).
  - [25] C. A. Ku-Leh et al., *Phys. Rev. B* 71, 205211 (2005).
  - [26] The CP amplitude in 3(b) was calculated by taking the peak height of the maxima of the probe profile, assuming it occurs at the inflection point of a Lorentzian function centered at the second excitonic transition for a given ( $n,m$ ) semiconducting nanotube with a halfwidth at half maximum of 30 meV, and setting it equal to the expression for the first derivative of the Lorentzian function.
  - [27] M. Cardona, *Modulation Spectroscopy* (Academic Press, New York, 1969).